Quantum fluctuations in unstable dissipative systems

S. T. Gevorkyan, G. Yu. Kryuchkyan, and N. T. Muradyan
Institute for Physical Research, National Academy of Sciences, Ashtarak-2, 378410, Armenia
(Received 1 June 1999; revised manuscript received 28 September 1999; published 13 March 2000)

We show how quantum instability is displayed in the von Neumann entropy and in the Wigner function. For this purpose, an intracavity second-harmonic generation close to the Hopf bifurcation range is studied. We examine the role of dissipation in unstable dynamics and the formation of the quantum states of the cavity modes, and discuss contrast ensemble behavior with that of individual realization on the basis of a quantum-jump simulation method. Namely, it is found that the Wigner functions for fundamental and second-harmonic modes prepared initially in a vacuum state acquire the three-hump structure due to phase symmetry breaking in the bifurcation range. The time evolution of coherent states leads to long-lived swing of the system between two side humps in a phase space.

PACS number(s): 42.50.Lc

I. INTRODUCTION

Environment coupled to a quantum system leads to dissipation, i.e., to irreversible loss of energy and coherence, and can monitor some of the system observables. As a result, the eigenstates of the system observables decohere and behave like the classical states. The coupling to the environment also degrades the squeezed states of the radiation field and destroys the quantum-mechanical interference effect. As a result, a linear superposition of macroscopically distinct quantum states are reduced to a statistical mixture [1–3]. Decoherence time for macroscopic objects is typically many orders of magnitude shorter than any other dynamical time scale. Therefore, the stability of quantum superposition states requires methods for slowing down the decoherence. Several proposals have been given in the literature [4–7]. Namely, it has recently been shown that couplings to the environment with a certain symmetry can lead to slow decoherence [8–10]. Note that the experimental testing of decoherence has been recently initiated [11]. In the context of the quantum to classical transition, decoherence makes the quasiclassical limit of such open systems both more realistic and simpler in many respects than the more familiar quasiclassical limit for isolated systems. These and other properties of dissipative quantum systems are well established for the regimes of stable time evolution but are insufficiently studied for nonlinear systems involving bifurcations and ranges of instabilities, where the dynamics strongly depends on any possible small fluctuations of environment.

In the present paper, our purpose is to investigate the role of dissipation due to the quantum fluctuations of the electromagnetic field in the context of quantum unstable systems—the systems having instability in the classical limit. Especially we wish to study the evolution of quantum noise in unstable nonlinear dynamics and adjacent questions of forming the quantum states in the ranges of bifurcations on the frame of Wigner functions. These investigations are complemented by consideration of quantum information aspects of nonlinear dynamics with the instability.

As a nonlinear system involving instability we consider the phenomenon of frequency doubling, i.e., second-harmonic generation (SHG) in a cavity, because it displays rich variety of classical nonlinear dynamics and has well understood quantum-mechanical description. This system is characterized by Hopf bifurcation which connects a steady-state regime to a temporal periodic regime. Intracavity frequency doubling consists in transformation, via a $\chi^{(2)}$ nonlinear crystal, of an externally driven fundamental mode with the frequency ω_1 into the second-harmonic mode with the frequency $\omega_2=2\omega_1$ $(\omega_1+\omega_1\rightarrow\omega_2)$. It was shown in Ref. [12], that the steady-state regime of SHG is realized only for relatively small intensities of the driving field. Beyond the critical value E_{cr}

$$E_{cr}=(2\gamma_1+\gamma_2)\left[\frac{2\gamma_2(\gamma_1+\gamma_2)}{k^2}\right]^{1/2} \tag{1}$$

(where γ_1 and γ_2 are the cavity damping rates, and k is the coupling constant proportional to the second-order susceptibility $\chi^{(2)}$) of the driving field and in the semiclassical approximation, without consideration of quantum noise, the intensities of the fundamental and second-harmonic modes demonstrate self-pulsing temporal behavior [13,14]. The self-pulsing takes place even when the cavity is resonant both at the fundamental and second-harmonic modes. The Hopf bifurcations are also observed for intracavity third-harmonic generation [15]. For detuned configuration other phenomena such as period doubling and chaos have been also predicted [16]. In Ref. [17], the stability of the steady-state solutions was analyzed for a model of a frequency-doubler laser. Recently the models of cascaded intracavity doubling involving two- and three-Hopf bifurcations were presented in Ref. [18]. The applications of self-pulsing phenomena can be found in Refs. [19,20,22].

The system of interest is dissipative because light is lost through the partially transmitting mirrors of the cavity. This loss is modeled by coupling the cavity modes to reservoir. It is known that consistent quantum theory of nonlinear interaction of radiation field modes in the cavity is based on the Fokker-Plank equation for quasiprobability distribution or on equivalent Langevin equations for stochastic amplitudes (see, e.g., Ref. [21]). In most theoretical works, however, the nonlinear systems are usually described within the linear treatment of quantum fluctuations, where the common definition of a bifurcation as a critical point in nonlinear optical

system emerged from the analysis of semiclassical solutions and their stability regions. In this sense the semiclassical dynamics of the fundamental and second-harmonic modes in intracavity SHG is associated with the Hopf bifurcation of the phases of two modes at the critical value of driving field E_{cr} 1. Note also that for the SHG involving Hopf instability, the linear treatment can be formulated as the evolution equations for the field fluctuations linearized around a periodic self-pulsing deterministic solution [22]. Clearly, linearized theories are limited in scope and, in particular, do not describe the critical region, where levels of quantum noise are usually very high. At the same time finding the quasiprobability distributions is extremely difficult and the solutions of the Fokker-Plank equation, which are exact in quantum fluctuations, have been established only for relatively simple systems but not for SHG (see, e.g., Ref. [23] and references therein). Recently, new descriptions of open systems in terms of state vector trajectories have been proposed using quantum-state diffusion [24] or quantum-jump model [25,26].

It should be noted, that quantum numerical investigations of SHG have been performed by a number of authors. The quantum dynamics of photon numbers for SHG in the instability range using the method of numerical solutions of Langevin's stochastic equations was first investigated in Ref. [27]. More recently, in the studies of dynamics of photon number in SHG, both the quantum-state diffusion (QSD) method [24,28] and QSD with a moving basis [29] were employed. The application of the quantum-jump method to SHG was performed in Ref. [30]. Most of the cited papers are devoted to numerical studies of the dynamics of photon numbers. The numerical investigation of the joint distributions for photon numbers and phases of the interacted modes has been presented in Ref. [31] for SHG and in Ref. [32] for third-harmonic generation.

Our analysis of intracavity SHG is based on the quantum-jump simulation method also known as the state-vector Monte Carlo method, and is devoted to the studies of the Wigner function and the entropy of each of the modes. This method considers not the density matrix but deals with state vector $|\Phi^{(\alpha)}(t)\rangle$ which is a member of an ensemble of state vectors.

As a measure of the entanglement and dissipation we use the von Neumann entropies of the modes which are defined through their respective reduced density operators as

$$S_j = -\mathrm{Tr}_j(\rho_j \ln \rho_j), \tag{2}$$

where the subscript $j=1,2$ is taken to imply the modes. This entropy is a sensitive operational measure of the quantum correlation, quantum information, and entanglement of both isolated or open systems, as well as the measure of the purity of quantum state [33,34]. If the system is in pure state the entropy [Eq. (2)] is precisely zero.

It should be noted that in most studies, the photon entanglement mechanism is imposed by spontaneous radiative processes, namely, on cascade transition in an atom or down-conversion in a nonlinear medium. In the system of interest, entanglement is realized between the fundamental and second-harmonic modes involved in nonlinear dynamics with the Hopf bifurcation. We incorporate these studies of the entropy with the analysis of the Wigner functions of both the modes for problems of quantum instability in SHG close to the bifurcation range. We will discuss the contrast between the ensemble behavior of the open system and instability dynamics of an individual realization. For this, the quantum simulation shown below, on the basis of the quantum-jump approach, will refer to the ensemble-averaged time evolution of the Wigner functions as well as to the time evolution of single realizations. We restrict ourselves to the numerical simulation of the stochastic dynamics in the quantum regime where the number of photons in the modes required to reach the Hopf bifurcations is less than $n=20$.

The outline of this paper is as follows. In Sec. II we describe in more detail the nonlinear system under consideration and show how the master equation can be studied using a Monte Carlo quantum-jump approach. Section III combines the numerical results for dynamics of the entropy and Wigner functions when the initial state of the modes is the vacuum state. Section IV is devoted to the evolution of the coherent states. Finally, Sec. V gives a summary of the main results.

II. QUANTUM-JUMP APPROACH FOR FREQUENCY DOUBLING

We consider doubly resonant SHG in which two photons with the frequency $\omega_1=\omega$ in the fundamental mode a_1 can annihilate to produce a photon with the frequency $\omega_2=2\omega$ in the second-harmonic mode a_2. The fundamental mode is driven by an external classical field with the amplitude E. This model is described by the following Hamiltonian in the interaction picture:

$$H_{sys} = i\frac{\hbar k}{2}(a_1^{\dagger 2}a_2 - a_1^2 a_2^\dagger) + i\hbar(Ea_1^\dagger - E^* a_1), \tag{3}$$

where k is the coupling constant proportional to the second-order susceptibility $\chi^{(2)}$. The losses in the input-output cavity mirror are accounted for by means of independent reservoir interaction for each mode. If we are interested only in the subsystems of two modes we must trace over the reservoir to obtain the density matrix for the subsystem ρ. Taking the trace over the reservoir in the Born-Markov approximation the corresponding master equation in the Lindblad form is obtained

$$\frac{\partial \rho}{\partial t} = -\frac{i}{\hbar}[H_{sys},\rho] + L\rho,$$
$$L\rho = \sum_{i=1}^{2} \gamma_i (2a_i \rho a_i^\dagger - \rho a_i^\dagger a_i - a_i^\dagger a_i \rho). \tag{4}$$

This equation describes the fundamental and second-harmonic modes decaying in the cavity and γ_i are the cavity damping rates.

We now briefly explain the quantum-jump simulation approach to the system considered using the general results

presented in Ref. [25]. The vector of the system which is one member of an ensemble of state vectors is expressed in the Fock basis of two modes as

$$|\Phi^{\alpha}(t)\rangle=\sum_{m,n}^{N} a_{mn}^{(\alpha)}(t)|m\rangle_1|n\rangle_2, \tag{5}$$

where the index α indicates the realizations and $|m\rangle_1$ and $|n\rangle_2$ are the Fock states of the fundamental and the second-harmonic modes. Note, that the coefficients $a_{mn}^{(\alpha)}(t)$ depend on the indexes of both modes simultaneously but not on the photon number of each mode separately.

The density matrix of the system is calculated as mathematical expectation of the matrixes of these pure states

$$\rho(t)=M\{|\Phi^{\alpha}(t)\rangle\langle\Phi^{\alpha}(t)|\}=\lim_{N\to\infty}\frac{1}{N}\sum_{\alpha}^{N}|\Phi^{\alpha}(t)\rangle\langle\Phi^{\alpha}(t)|, \tag{6}$$

N is the number of independent realizations.

The reduced density operators for each of the modes are constructed from the full density operators ρ by tracing over the other mode. Thus,

$$\rho_{1(2)}=\mathrm{Tr}_{2(1)}(\rho) \tag{7}$$

and in the Fock basis we find

$$\rho_{1,nm}(t)=M\left\{\sum_{q}^{N} a_{nq}^{(\alpha)}(t)a_{mq}^{*(\alpha)}(t)\right\}, \tag{8}$$

$$\rho_{2,nm}(t)=M\left\{\sum_{q}^{N} a_{qn}^{(\alpha)}(t)a_{qm}^{*(\alpha)}(t)\right\}. \tag{9}$$

The procedure adopted in the quantum-jump simulation for the system Hamiltonian (3) consists of the following. The evolution of the one member of the ensemble of pure states $|\Phi^{(\alpha)}(t)\rangle$ over a short time δt if there is no quantum jump is governed by the non-Hermitian effective Hamiltonian

$$H_{eff}=H_{sys}-\frac{i\hbar}{2}(\gamma_1 a_1^{\dagger}a_1+\gamma_2 a_2^{\dagger}a_2). \tag{10}$$

The calculation at first order of δt for the amplitudes $a_{mn}(t)$ gives the following formula:

$$\begin{aligned}a_{mn}(t+\delta t)=\frac{1}{\sqrt{1-\delta p}}\Bigg\{&a_{mn}(t)\left[1-m\frac{\gamma_1\delta t}{2}-n\frac{\gamma_2\delta t}{2}\right]\\&+\delta tE\sqrt{m}a_{m-1,n}(t)-\delta tE^{*}\sqrt{m+1}a_{m+1,n}(t)\\&+\frac{k\delta t}{2}[\sqrt{m(m-1)(n+1)}a_{m-2,n+1}(t)\\&-\sqrt{n(m+1)(m+2)}a_{m+2,n-1}(t)]\Bigg\},\end{aligned} \tag{11}$$

where

$$\delta p=\delta p_1+\delta p_2, \tag{12}$$

and

$$\delta p_1=\delta t\,\gamma_1\sum na_{nm}(t)a_{nm}^{*}(t), \tag{13}$$

$$\delta p_2=\delta t\,\gamma_2\sum na_{mn}(t)a_{mn}^{*}(t). \tag{14}$$

Such evolution must be completed by the possibility of quantum jump. This quantum jump theory, unlike the single mode case, contains two jump operators a_1 and a_2, therefore the jumps change the photon numbers of both the modes. In the case of the emission of a photon from the fundamental or the second-harmonic modes the state vector is jumped as

$$|\Phi(t)\rangle\to\frac{\sqrt{\gamma_1}a_1|\Phi(t)\rangle}{\sqrt{\delta p_1/\delta t}} \tag{15}$$

or

$$|\Phi(t)\rangle\to\frac{\sqrt{\gamma_2}a_2|\Phi(t)\rangle}{\sqrt{\delta p_2/\delta t}}, \tag{16}$$

with the probabilities $\delta p_1/\delta t$ and $\delta p_2/\delta t$. In accordance with Eqs. (15) and (16) the amplitudes of photon numbers are changed as

$$a_{mn}(t+\delta t)=\frac{a_{m+1,n}(t)\sqrt{m+1}}{\left[\sum_{m,n} na_{nm}(t)a_{nm}^{*}(t)\right]^{1/2}}, \tag{17}$$

or

$$a_{mn}(t+\delta t)=\frac{a_{m,n+1}(t)\sqrt{n+1}}{\left[\sum_{m,n} na_{mn}(t)a_{mn}^{*}(t)\right]^{1/2}}. \tag{18}$$

In the following we shall focus on two kinds of initial states of both cavity modes. The cases of vacuum states and coherent states will be considered. We restrict ourselves to the numerical simulation of a set of state vectors at time t using truncated Fock basis as in the cited papers [24–26,28,30], and in the regime of strong nonlinearity. We have also used the state vector Monte Carlo method to determine Wigner functions for the quantum states of modes during the time evolution. For this goal we apply the method presented in Ref. [10]. Generalizing this method for the case of two modes we express the Wigner functions for both the fundamental and second-harmonic modes in the following form:

$$W_i(r,\theta)=\sum_{m,n}\rho_{i,mn}W_{mn}(r,\theta), \tag{19}$$

$(i=1,2)$, (r,θ) are the polar coordinates in the complex phase-space plane $X=r\cos(\theta)$, $Y=r\sin(\theta)$ and the coeffi-

cients $W(r,\theta)$ are Fourier transforms of matrix elements of the Wigner characteristic function

$$W_{mn}(r,\theta)=\begin{cases}\dfrac{2}{\pi}(-1)^n\sqrt{\dfrac{n!}{m!}}e^{i(m-n)\theta}(2r)^{m-n}e^{-2r^2}L_n^{m-n}(4r^2), & m\geqslant n\\ \dfrac{2}{\pi}(-1)^m\sqrt{\dfrac{m!}{n!}}e^{i(m-n)\theta}(2r)^{n-m}e^{-2r^2}L_m^{n-m}(4r^2), & n\geqslant m\end{cases} \tag{20}$$

with L_p^q being the Laguerre polynomials.

III. TIME EVOLUTION OF VACUUM MODES: ENSEMBLE BEHAVIOR AND INDIVIDUAL REALIZATIONS

Before discussing the quantum instability let us briefly comment on the transition of the system from stable dynamics to unstable. In the semiclassical approximation, which means ignoring the noise terms, the stability takes place below the critical point. In this range and in the steady-state regime ($\gamma_{1,2}\gg 1$) the photon numbers n_i and phases φ_i ($i=1,2$), of the fundamental and second-harmonic modes are determined by the following expressions [12]:

$$n_1=2\frac{\gamma_2}{k}\sqrt{n_2},\quad E/\gamma_1=\sqrt{n_1}\left(1+\frac{k}{\gamma_1}\sqrt{n_2}\right), \tag{21}$$

$$\varphi_1=\phi,\quad \varphi_2-2\varphi_1=\pi, \tag{22}$$

where ϕ is the phase of the pump field. Beyond E_{cr} the dynamics of photon numbers of the modes moves to the self-pulsing regime. The physical reason for self-pulsing is the instability of the phases of the cavity fields. This problem has been recently analyzed quantum mechanically using Langevin's stochastic equation of motion. In particular, it has been shown [31] from ensemble-averaged simulation, that the most probable values of phases in each of the modes and in a fixed moment of time has zero value below the critical range and branches into two symmetrically situated values when a system moves through the critical range.

We shall give the results of the quantum-jump analysis of SHG using expansion of the state vectors in the Fock state basis of the two modes (5). For simplicity of analysis we take $\gamma_1=\gamma_2=\gamma$ and introduce the dimensionless parameters as

$$\varepsilon\equiv E/\gamma,\quad g\equiv k/\gamma,\quad \tau\equiv\gamma t. \tag{23}$$

In order to choose a truncated basis of two modes we concretize the operational regime. The usual situation in quantum optics is to operate in the regime of weak nonlinearity for which $g\ll 1$, so that $\varepsilon_{cr}\gg 1$. Then the system is able to reach the Hopf bifurcation if the fundamental cavity mode is driven by a high intensity coherent field. This leads to large photon number in the modes. However, it is difficult to obtain a single quantum trajectory in this regime, not to mention performing an ensemble average. In the following we consider the regime of strong nonlinearity, $g=0.6$, and vary the value of the external field. It means the strong nonlinear coupling between two fundamental and second-harmonic modes but not the strong coupling of cavity modes to reservoir, so that the Born-Markov approximation is valid. This regime is strongly quantum mechanical, as in the vicinity of Hopf bifurcation the maximum photon number in both the modes is less than 20, if $\varepsilon=6$, for instance (see below, Fig. 1). Note that in the regime considered the mean photon numbers of fundamental and second-harmonic modes approximately equal each other. For large values of relative nonlinearity g the dynamics of the modes is characterized by a broad critical range of the driving field amplitude instead of the bifurcation point which is equal to $\varepsilon_{cr}=10$, for $\gamma_1=\gamma_2=\gamma$ and $g=0.6$. We note that the system with such extremely large nonlinearities is far to be realized in practice and here we do not intend to give results close to an experimental situation but discuss the fundamental problems of quantum instability for the simplest model. Note that similar strong nonlinearity regimes were considered by quantum simulation methods in most of the cited papers [24,28].

At first, we chose the vacuum state as the initial state of both modes and analyzed the individual time-dependent realizations to find the range of instability. The basis is $n=20$ number states for each mode for a total size of 20^2

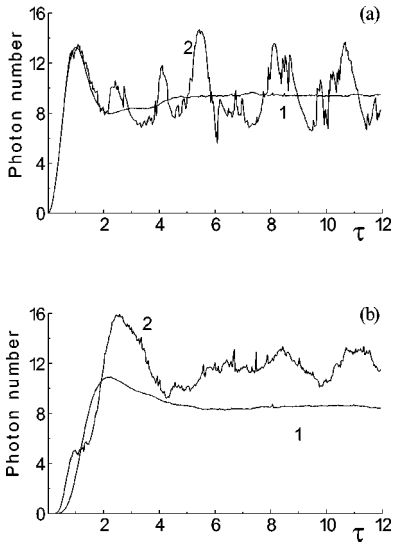

FIG. 1. The time evolution of the mean photon numbers of the fundamental (a) and second-harmonic mode (b) prepared initially in the vacuum state, ensemble averaged over 1000 realization (1) and an individual realization (2). The parameters are $\gamma_1/\gamma_2=1$, $g=0.6$, $\varepsilon=6$.

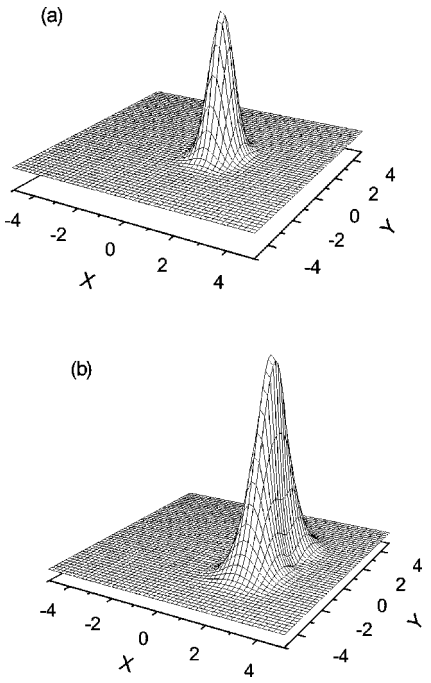

FIG. 2. The Wigner functions of the fundamental mode prepared initially in the vacuum state for $\varepsilon=1$ (a) and $\varepsilon=3$ (b) and for $\tau=8$; averaged over 150 realizations.

states. In Fig. 1 we illustrate the time evolution of the photon numbers averaged over 1000 single trajectories. These figures show that the mean photon numbers of both modes (curves 1) reach the stationary values. At the same time, as the calculations show, each of the time-depended trajectories of the photon numbers (curves 2) strongly depends on the realization and shows oscillations which indicate the self-pulsing temporal behavior. However, the oscillations are almost reduced by averaging over the ensemble. This results are in accordance with the analogous results of quantum simulation obtained on the basis of Langevin equations [27,28]. The difference is that here we study the unstable dynamics of modes in the critical range of the system. On the whole we find more effective quenching of the self-pulsing of individual trajectories due to their averaging over ensemble than in Ref. [27]. Nevertheless, we will clearly see below the properties of instability in the frames of both the entropy and the Wigner function for the same parameters, as in Fig. 1.

A. Entropy and Wigner function in the vicinity of Hopf bifurcation

In connection with the above results the following interesting question arises on how the self-pulsing instability in the nonlinear system under consideration is displayed in quantum ensemble theory. To answer this question we consider the von Neumann entropies and the Wigner functions of the fundamental and second-harmonic modes, which provide a large amount of information about the states of the modes and also provide a pictorial view. We calculate the evolution of the entropy by formula (2) using the results for reduced density matrixes (8), (9) expressed through the ensembles of trajectories. The calculations were performed by diagonalization of the matrix $\rho_{1(2),nm}$ in the Fock states basis. The Wigner function is calculated by formulas (19) and (20).

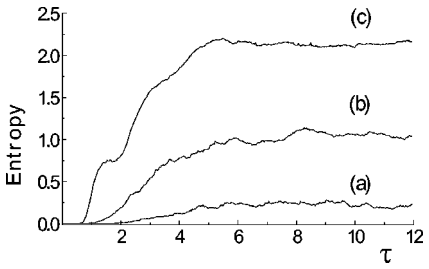

FIG. 3. The time evolution of the entropy of the fundamental mode prepared initially in the vacuum state for $\varepsilon=1(a)$, over 150 realizations; $\varepsilon=3(b)$, over 150 realizations; $\varepsilon=6(c)$, over 1000 realizations.

Now we present the ensemble-averaged results which contain 1000 realizations by using the state vector Monte Carlo simulation combining the studies of entropy and Wigner function. In Fig. 2 we demonstrate moving our system within the range of stable generation to the bifurcation range by plotting the Wigner function for two values of driving field: $\varepsilon=1$ (a) and $\varepsilon=3$ (b) in a fixed moment of time. On the left of bifurcation, Fig. 2(a) shows transformation of the initial vacuum state to the state close to the pure coherent state. When we move into the bifurcation range by increasing the intensity of the pump field, this state becomes squeezed, which is displayed as the squeezing of Gaussians [Fig. 2(b)]. The Wigner function is single humped and centered at $X=1.5$ and $Y=0$. We find that during the whole time, after the transient time $\tau\geqslant 5$, behavior of the states (Fig. 2) remains without any modifications.

The simulation results of the time evolution of the entropies are plotted in Figs. 3 and 4 for various values of the driving field $\varepsilon=1(a)$; $3(b)$; $6(c)$. We see that the entropies of both modes reach the stationary values. We note that even for $\varepsilon=1$, when the system is far from the bifurcation point, the modes are not in pure states. The reason is the entanglement of modes due to the nonlinear interaction between them and feedback effects, as well as dissipation. We see increasing of the entropy with increasing the intensity of the driving field when the system moves to the bifurcation range.

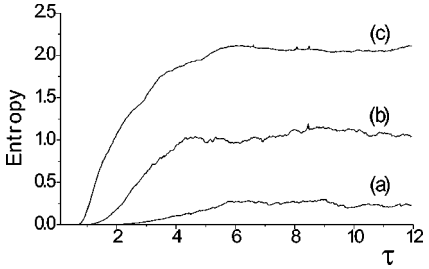

FIG. 4. The time evolution of the entropy of the second-harmonic mode prepared initially in the vacuum state for $\varepsilon=1(a)$, over 150 realizations; $\varepsilon=3(b)$, over 150 realizations; $\varepsilon=6(c)$, over 1000 realizations.

Now we present in more detail the results on the bifurcation range. The ensemble-averaged results for the Wigner function are shown in Fig. 5. We see from these figures and also from Figs. 3(c) and 4(c) that the modes are in the pure states for small times $\tau \lesssim 0.7$, where the entropies are equal to zero. In Fig. 5(a) the modes start at $\tau=0$ in the vacuum state which is Gaussian in the phase-space plane centered at $X=Y=0$. The Wigner functions at $\tau \simeq 0.7$ are situated symmetrically in the phase-space plane and indicate that both the modes are in pure coherent states, Figs. 5(b) and 5(c). The further evolution of the system leads to the increasing of the entropies that means the forming of entangled states. The Wigner functions in Figs. 5(d) and 5(e) at time $\tau \simeq 1.67$ are single humped and show the action of the squeezing processes in the SHG, which is displayed as the squeezing of Gaussians (see Sec. III C). Then the time evolution of entropies as well as the Wigner functions becomes stationary stable. We can see the formation of the entangled states of both the fundamental and the second-harmonic modes which are represented in the Wigner functions Figs. 5(f) and 5(g) as the appearance of two additional side humps. It is natural to connect the occurrence of the side humps with the unstable dynamics of the phases in the semiclassical limit of the intracavity SHG. As mentioned above, in quantum treatment the Hopf instability is looked at as the splitting of both the most probable values of phases into two symmetrically situated values. With increasing E we enter into the critical transition domain, in the vicinity of the Hopf bifurcation, where a spontaneous breaking of the phase symmetry occurs. We suppose that two side humps of the Wigner functions display the states of each of the modes with equal intensities and opposite phases.

The time evolution of the entropies of the modes reflects the time evolution of the degree of entanglement between the modes. We note that in the vicinity of the Hopf bifurcation the entropy production for long times $\tau \gtrsim 6$ gives the relatively high values. It is useful to compare these values of the entropy with those that take place for some well-known mixed states. As we see from Figs. 1(a) and 3(c) the entropy production for long times gives $S_1=2.2$ for the mean photon number of the fundamental mode equal to $n_1=9$. It is easy to check that for the same value of the mean photon number the entropy of the one-mode thermal mixed state is equal to $S=3.3$, while the entropy of the phase-averaged coherent state is equal to $S=2.5$. This fact, if we consider the maximal value of the entropy as $\ln N$, where N is the effective number of the states of the modes, allows us to suppose that each of the two side humps of the Wigner functions displays the mixtures of pure states which are not resolved. In this way Figs. 5(f) and 5(g) portray the quantum interference between these two components, i.e., the quantum interference between two groups of close states. This statement needs special investigation, nevertheless, the additional arguments in favor of this point of view will be presented below by considering the individual trajectories.

B. Peculiarities of individual realizations

In this section we address the question of how an individual realization evolves in the regime of quantum instability. For this goal we plot in Figs. 6(a) and 6(b) the two possible realizations of the Wigner function. We observe that these realizations as well as all others are strikingly different from the ensemble-averaged results (Figs. 5). As a rule the samples obtained contain the interference fringes between two components. The other interesting feature is that each realization, without exception, of the ensemble evolves to the two components (groups of states) with quantum interference between them. This fact confirms the above statement relative to the quantum interference in the ensemble-averaged Wigner function. In reality, in the other case of statistical mixtures between two components, the same realizations with one of the components could be possible. So, the analysis of individual realizations of the Wigner functions (Fig. 6) shows that on the range of bifurcation the system is delocalized in its two components due to coupling with a dissipative environment, which is the electromagnetic reservoir.

It is useful also to present the results concerning the quadrature amplitudes. As we know the probability distribution $P(X,\phi)$ for any quadrature amplitude operator $X_\phi = [a\exp(-i\phi)+a^\dagger \exp(i\phi)]/2$ can be obtained by integrating of the Wigner function over the conjugate quadrature [35,36]

$$P(X,\phi)=\int_{-\infty}^{+\infty} dp\, W(X\cos\phi - p\sin\phi, X\sin\phi + p\cos\phi). \tag{24}$$

In Figs. 5 and 6 the projections of the Wigner functions on the X and Y axes describe the marginal distributions $P(X)=P(X,0)$ and $P(Y)=P(X,\pi/2)$. As we clearly see in Fig. 6, $P(Y)$ distributions for a single realization as well as ensemble-averaged distributions in Fig. 5 are symmetrical relevant to zero. Therefore it seems that the arbitrary time-dependent individual realization of $Y=X_{\pi/2}$ quadrature component

$$Y^{(\alpha)}(t)=\int P^{(\alpha)}(Y,t)\,Y\,dY \tag{25}$$

is equal to zero over all times. Really, it is also confirmed directly by quantum-jump simulation. It is known that the quadrature amplitudes Y_1 and Y_2 of two modes describe the phase properties of the system. We remind in this connection that the phase of the pump field was taken equal to zero in our numerical analysis as well as the phase of the initial vacuum state. Therefore, the result $Y_1^{(\alpha)}(t)=Y_2^{(\alpha)}(t)=0$ means that the phases of the modes remain invariable during the quantum-jump evolution. The results of evolution of the single realizations of the orthogonal quadrature components $X_1^{(\alpha)}(t)$ and $X_2^{(\alpha)}(t)$ are shown in Fig. 7. These results of the numerical simulations of the quadrature components are different from the results obtained in Ref. [37] on degenerate three-photon down-conversion. The mentioned system is classically stable and as shown in Ref. [37] by the quantum trajectory simulation, the state vector well localized in phase space. The system spends most of its time close to one of the classical solutions, with tunneling events occurring at random intervals in contrast to the time evolution depicted on Fig. 7.

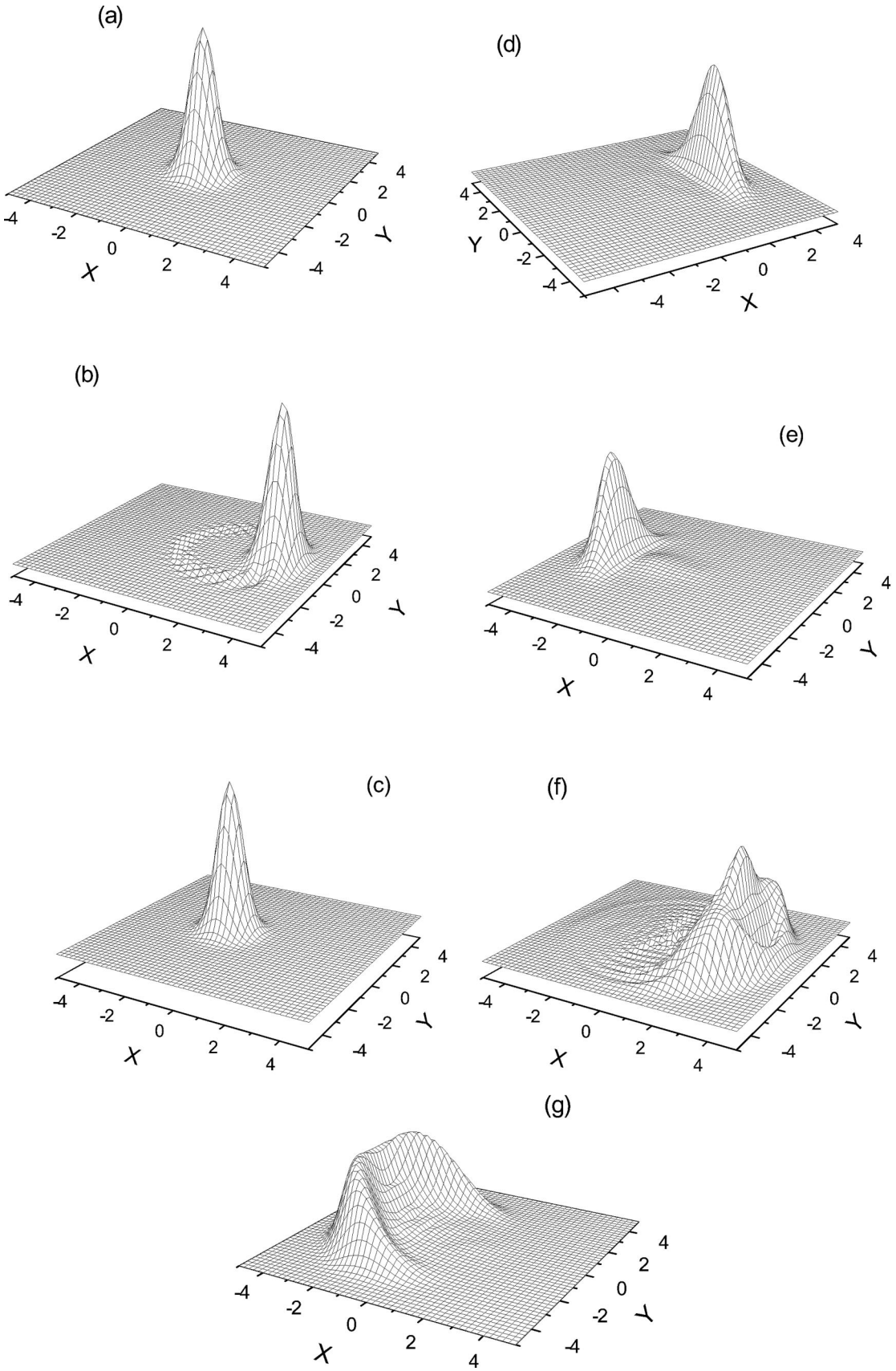

FIG. 5. The Wigner functions at $t=0$ (the same for both the modes) (a); $\tau=0.7$ of the fundamental mode (b) and second-harmonic mode (c); $\tau=1.67$ of the fundamental mode (d) and second-harmonic mode (e); $\tau=8.9$ of the fundamental mode (f) and second-harmonic mode (g) and for $\varepsilon=6$, averaged over 1000 realizations.

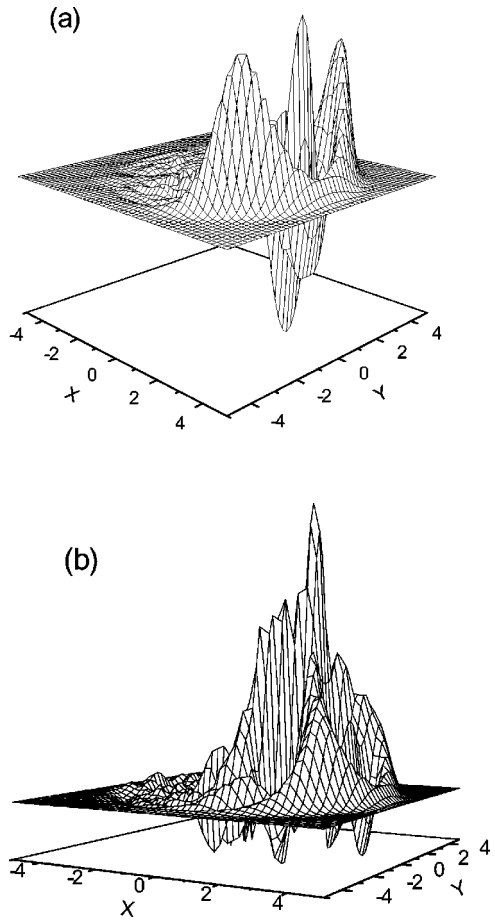

FIG. 6. The Wigner functions of an individual realizations (a), (b) for the fundamental mode prepared initially in the vacuum state and for $\varepsilon=6$.

C. Ensemble-averaged quadrature variances

As we noted, the Wigner functions in Figs. 2(b), 5(d), and 5(e) show squeezing properties of the quadrature distributions $P_{1,2}(X)$. We now verify this statement by actual calculations of the quadrature variances. The results for the time evolution of the variances defined as

$$\Delta X_{1,2}(t)=\sqrt{\langle X_{1,2}^2(t)\rangle-\langle X_{1,2}(t)\rangle^2}, \tag{26}$$

for $X_i=(a_i+a_i^{\dagger})/2$, $i=1,2$ are given in Fig. 8. These results correspond to the parameter $\varepsilon=3$ and have been obtained

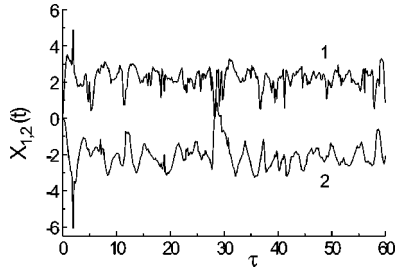

FIG. 7. The time evolution of the orthogonal quadrature components $X_1(t)$ (1) and $X_2(t)$ (2) of the modes prepared initially in the vacuum state and for $\varepsilon=6$.

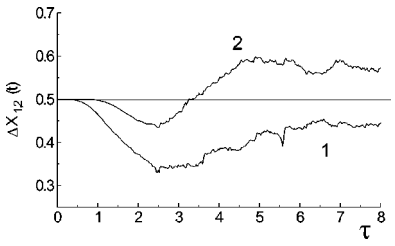

FIG. 8. The time evolution of the variances $\Delta X_{1,2}(t)$ for fundamental (curve 1) and second-harmonic modes (curve 2) and for $\varepsilon=3$.

with the average of 100 trajectories. In Fig. 8 we clearly see the existence of quadrature squeezing of the fundamental mode for long time intervals in accordance with the behavior of the Wigner function [Fig. 2(b)]. The squeezing is maximal $\Delta X_1\simeq 0.32$ for $\tau\simeq 2.5$. As the calculations show, the squeezing decreases when we move into the bifurcation range. So, for $\varepsilon=6$ the maximal squeezing for fundamental mode $\Delta X_1\simeq 0.42$ at $\tau\simeq 1.9$ and for second-harmonic $\Delta X_2\simeq 0.48$ at $\tau\simeq 0.9$.

IV. ANTIPHASE QUANTUM DYNAMICS FOR COHERENT-STATE EVOLUTION

So far we have analyzed the quantum instability in SHG assuming the initial states of both the modes as the vacuum state. Such an initial condition is natural for the intracavity SHG and has been realized in most of the experiments. However, the above investigation is insufficient for the full consideration of the fundamental problems of an instability. In particular, it is interesting to analyze in more detail the phase properties of the self-pulsing phenomena using the quantum-jump simulation. For this goal we consider in this section the other scenario of the nonlinear dissipative evolution when cavity modes are initially prepared in the coherent states $|\alpha_1\rangle$ and $|\alpha_2\rangle$. We operate with the special case of the states having the same intensities, but the opposite values of phases $\alpha_1=e^{i\pi}\alpha_2=\sqrt{|\alpha|^2}e^{i\varphi}$.

It is found that the time evolution of ensemble-averaged quadrature amplitudes and Wigner functions have nonstationary behavior different from the case of vacuum modes evolution. At first in Fig. 9 we show the time dependence of ensemble-averaged quadrature phase components $\langle Y_1\rangle$ and $\langle Y_2\rangle$ which initially equal $\langle Y_1(0)\rangle=-2$, $\langle Y_2(0)\rangle=2$. As we see, each of the quadrature amplitudes displays oscilla-

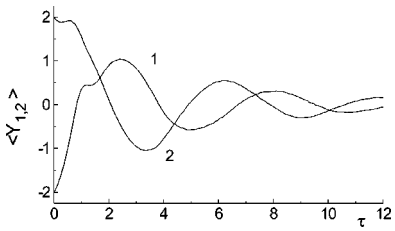

FIG. 9. The time evolution of ensemble-averaged quadrature components $\langle Y_1\rangle$ (curve 1) and $\langle Y_2\rangle$ (curve 2) for initial coherent states of the modes with $\alpha_1(t=0)=-2i$, $\alpha_2(t=0)=2i$, and parameters $\gamma_1/\gamma_2=1$, $g=0.6$, $\varepsilon=6$, over 1000 realizations.

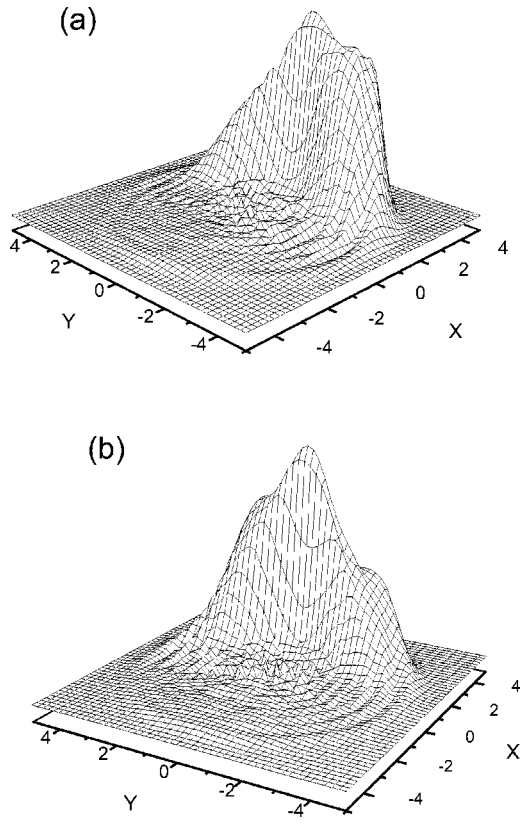

FIG. 10. Ensemble-averaged over 1000 realizations Wigner functions of the fundamental mode prepared initially in the coherent state with $\alpha_1(t=0)=-2i$, $\alpha_2(t=0)=2i$ at $\tau=4.9$ (a) and $\tau=8.2$ (b) and $\varepsilon=6$.

tions, with a phase correlation between them. Such a property of nonlinear systems oscillating with a strong phase correlation is called antiphase dynamics and was well established for the self-pulsing state of intracavity SHG without dissipation [17]. As we have shown, on the basis of quadrature amplitudes, the dissipation leads to the damping of oscillations during time intervals longer than the photon lifetimes in the cavity.

Analogous nonstationary behavior is found also for the Wigner functions. In Fig. 10 we present the samples of ensemble-averaged Wigner functions of the fundamental mode at the time moments $\tau=4.9$ and $\tau=8.2$, which correspond to the minimum and maximum of $\langle Y_1(t)\rangle$, respectively. As we see for the evolution of coherent states, the peaks of the Wigner functions have different heights, unlike the previous case of the vacuum states evolution. Moreover, in the range of Hopf bifurcation, the system swings between these two components.

V. CONCLUSIONS

In conclusion, we have demonstrated the origin of quantum instability in an intracavity SHG using the quantum-jump simulation method. We have analyzed the von Neumann entropy and the Wigner function of the fundamental and second-harmonic modes in the vicinity of the Hopf bifurcation. Our calculations are performed for both the stable generation range and in the critical operational range of SHG, where quantum noise level essentially increases. This critical range emerges in the quantum treatment of the instability instead of the Hopf bifurcation point in the semiclassical approach. We have found that the different time evolution scenario of the Wigner function is dependent on the pump field intensity and have shown that the cavity modes exhibit remarkable quantum features due to entanglement between them and dissipation. We have demonstrated the origin of quantum instability for two different evolutions of the cavity modes prepared initially in the vacuum state and in the coherent states. Namely, we have established the appearance of two additional side humps of the Wigner functions in the vicinity of the Hopf bifurcation as a reflection of the phase spontaneous symmetry breaking for the vacuum modes. For the initial coherent states of modes we have found the long-lived time-dependent oscillations of quadrature amplitudes as well as the swing of Wigner function between two side humps. For a better illustration of these results we used the large ratio $k/\gamma=0.6$ in our numerical analysis. Unfortunately, we have not performed the quantum-jump simulation when the system moves through the Hopf bifurcation, which is an interesting, however, complicated option for the future.

ACKNOWLEDGMENTS

One of us (S.T.G.) wishes to acknowledge Professor A. Graham for useful questions and interesting comments during the investigation of quantum dynamics of unstable systems. One of us (G.Yu.K.) acknowledges helpful discussions with G. Alber, H. Carmichael, S. Fauve, I. Jex, W. Schleich, and K. Vogel. This work was supported in part by INTAS Grant No. 97-1672, and by the Armenian Science Foundation Grant Nos. 96-771 and No. 98-838.

[1] For an overview, see U. Weiss, *Quantum Dissipative Systems* (World Scientific Publishing, Singapore, 1993).
[2] E. Joss *et al.*, *Decoherence and the Appearance of a Classical World in Quantum Theory* (Springer, Berlin, 1996).
[3] W.H. Zurek, Phys. Scr. **76**, 186 (1998).
[4] J.F. Poyatos, J.I. Cirac, and P. Zoller, Phys. Rev. Lett. **77**, 4728 (1996).
[5] L. Viola and S. Lloyd, Phys. Rev. A **58**, 2733 (1998).
[6] D. Vitali, P. Tombesi, and G.J. Milburn, Phys. Rev. Lett. **79**, 2442 (1997).
[7] G. Vemuri, K.V. Vasavada, and G.S. Agarwal, Phys. Rev. A **50**, 2599 (1994).
[8] D.A. Lidar, I.L. Chuang, and K.B. Whaley, Phys. Rev. Lett. **81**, 2594 (1998).
[9] C.C. Gerry and E.E. Hach III, Phys. Lett. A **174**, 185 (1993).
[10] B.M. Garraway and P.L. Knight, Phys. Rev. A **49**, 1266

(1994).
[11] S. Haroche, Phys. Today **51**, 36 (1998).
[12] P.D. Drummond, K.J. McNeil, and D.F. Walls, Opt. Acta **27**, 321 (1980); **28**, 211 (1981).
[13] H.J. Kimble and J.L. Hall, in *Quantum Optics IV*, edited by J.D. Harvey and D.F. Walls (Springer, Berlin, 1986).
[14] S. Schiller and R. Byer, J. Opt. Soc. Am. B **10**, 1696 (1993).
[15] S.T. Gevorkyan, G.Yu. Kryuchkyan, and K.V. Kheruntsyan, Opt. Commun. **134**, 440 (1996).
[16] C.M. Savage and D.F. Walls, Opt. Acta **30**, 557 (1983).
[17] J.–Y. Wang and P. Mandel, Phys. Rev. A **48**, 671 (1993); **52**, 1472 (1995); X.–G. Wu and P. Mandel, J. Opt. Soc. Am. B **4**, 1870 (1987); J.–Y. Wang, P. Mandel, and T. Erneux, Quantum Semiclassic. Opt. **7**, 169 (1994); A.G. Vladimirov and P. Mandel, Phys. Rev. A **58**, 3320 (1998).
[18] G.Yu. Kryuchkyan, N.T. Mouradyan, and A.S. Sargsian, Opt. Commun. **146**, 208 (1998); K.V. Kheruntsyan, G.Yu. Kryuchkyan, N.T. Mouradyan, and K.G. Petrosyan, Phys. Rev. A **57**, 535 (1998); G.Yu. Kryuchkyan, S.H. Karayan, and N.T. Mouradyan, Opt. Commun. **159**, 309 (1998).
[19] P. Mandel and J.–Y. Wang, Opt. Lett. **19**, 533 (1994); E.A. Viktorov and P. Mandel, *ibid.* **22**, 1568 (1997).
[20] K. Germey, F.G. Schute, and R. Tiebel, Opt. Commun. **69**, 438 (1989).
[21] C.W. Gardiner, *Handbook of Stochastic Methods* (Springer, Berlin, 1986); D.F. Walls and G. J. Milburn, *Quantum Optics* (Springer, Berlin, 1996).
[22] N.T. Pettiaux, P. Mandel, and C. Fabre, Phys. Rev. Lett. **66**, 1838 (1991).
[23] G.Yu. Kryuchkyan and K.V. Kheruntsyan, Opt. Commun. **127**, 230 (1996); K.V. Kheruntsyan, D.S. Krähmer, G.Yu. Kryuchkyan, and K.G. Petrosyan, *ibid.* **139**, 157 (1997); G.Yu. Kryuchkyan, K.G. Petrosyan, and K.V. Kheruntsyan, Pis'ma Zh. Éksp. Teor. Fiz. **63**, 502 (1996) [JETP Lett. **63**, 526 (1996)].
[24] N. Gisin and I.C. Percival, J. Phys. A **25**, 5677 (1992); **26**, 2233 (1993); **26**, 2245 (1993).
[25] J. Dalibard, Y. Castin, and K. Molmer, Phys. Rev. Lett. **68**, 580 (1992); K. Molmer, Y. Castin, and J. Dalibard, J. Opt. Soc. Am. B **10**, 524 (1993).
[26] H.Y. Carmichael, *An Open Systems Approach to Quantum Optics*, Lecture Notes in Physics (Springer-Verlag, Berlin, 1993).
[27] M. Dörfle and A. Schenzle, Z. Phys. B: Condens. Matter **65**, 113 (1986).
[28] P. Goetesch and R. Graham, Ann. Phys. (Leipzig) **2**, 706 (1993).
[29] R. Schack, T.A. Brun, and I.C. Persival, J. Phys. A **28**, 1995 (1995).
[30] X.P. Zheng, C.M. Savage, Phys. Rev. A **51**, 792 (1995).
[31] S.T. Gevorkyan and W.H. Maloyan, J. Mod. Opt. **44**, 1443 (1997).
[32] S.T. Gevorkyan, Phys. Rev. A **58**, 4862 (1998).
[33] S.H. Barnett and S.J.D. Phoenix, Phys. Rev. A **40**, 2404 (1989); **44**, 535 (1991).
[34] L. Gilles, B.M. Garraway, and P.L. Knight, Phys. Rev. A **49**, 2785 (1995).
[35] H.J. Collett and D.F. Walls, Phys. Rev. A **32**, 2887 (1985).
[36] K. Vogel and H. Risken, Phys. Rev. A **40**, 2847 (1989).
[37] T. Felbinger, S. Schiller, and J. Mlynek, Phys. Rev. Lett. **80**, 492 (1998).